Materials Science-Poland, 35(4), 2017, pp. 861-867
http://www.materialsscience.pwr.wroc.pl/
DOI: 10.1515/msp-2017-0107

DE GRUYTER OPEN

Synthesis, characterization and photovoltaic properties of Mn-doped Sb_2S_3 thin film

SABIT HOROZ[1,*], OMER SAHIN[2]

[1]Siirt University, Faculty of Art and Sciences, Department of Physics, 56100, Siirt, Turkey
[2]Siirt University, Faculty of Engineering and Architecture, Department of Chemical Engineering, 56100, Siirt, Turkey

Synthesis and characterization of Mn-doped Sb_2S_3 thin films (TFs) prepared by chemical bath deposition (CBD) at room temperature have been documented and their structural, optical, morphological, magnetic and photovoltaic properties have been examined for the first time. Their structural properties reveal that the Mn-doped Sb_2S_3 TF has an orthorhombic phase structure of Sb_2S_3, and that the grain size of the Mn-doped Sb_2S_3 TF (72.9 nm) becomes larger than that of undoped Sb_2S_3 TF (69.3 nm). It has been observed that Mn content causes the Sb_2S_3 TF band gap to decrease. This situation clearly correlates with band tailing due to the impurities that are involved. The morphological properties have revealed that the shape of the Mn-doped Sb_2S_3 TF is more uniform than the shape of its undoped counterpart. The study on its magnetic properties has demonstrated that the Mn-doped Sb_2S_3 TF exhibits paramagnetic behavior. Its paramagnetic Curie-Weiss temperature was found to be −4.1 K. This result suggests that there is an anti-ferromagnetic interaction between Mn moments in the Mn-doped Sb_2S_3 TF. Incident photon to electron conversion efficiency (IPCE) and J-V measurements were also carried out for the Mn-doped Sb_2S_3 TF for the first time. The results have indicated that the Mn-doped Sb_2S_3 TF can be utilized as a sensitizer to improve the performance of solar cells. Another important observation on the photovoltaic properties of Mn-doped Sb_2S_3 TF is that the spectral response range is wider than that of undoped Sb_2S_3 TF. Our study suggests that the introduction of dopant could serve as an effective means of improving the device performance of solar cells.

Keywords: *characterization; chemical bath deposition (CBD); Mn-doped Sb_2S_3 thin films; photovoltaic properties*

1. Introduction

Much attention has been paid recently to synthesis and characterization of group V-VI semiconductors owing to their unique optical properties. Sb_2S_3, which has a direct band gap of 1.78 eV to 2.5 eV, has been extensively utilized as an important material in numerous industrial applications such as microwave devices, solar cells, various optoelectronics devices, and IR sensors. It is one of the most important $A_2{}^{V}B_3{}^{VI}$ metal chalcogenides due to its extraordinary physical and chemical properties [1–6].

Sensitized solar cells utilizing group V-VI semiconductors, can be used as sensitizers in semiconductor-sensitized solar cells, and are favorable materials for improving photovoltaic (PV) devices at a low-cost and with high performance. The undoped Sb_2S_3 thin films (TFs) have notable optical and electrical properties and can be employed as sensitizers [7–10]. Zhong et al. [11] performed a study that aimed to obtain high efficiency solar cells using undoped Sb_2S_3 thin films. They showed that Sb_2S_3-modified TiO_2 materials have a power conversion efficiency (PCE) that is enhanced by over 175 % and that exhibits a PCE of 2.32 %. Mushtaq et al. [12] reported that doped Sb_2S_3 TFs open new opportunities for research, as well as for the applications of nanostructured materials. They concluded that Ni-doped Sb_2S_3 TFs have higher absorption coefficient and refractive index values, and can be used for solar cell applications.

In addition to improving the efficiency of solar cell devices, the doped semiconductor TFs or nanoparticles (NPs), which have been termed as diluted magnetic semiconductors, can be used as desirable materials for spintronic applications [13]. The magnetic behavior of the semiconductor TFs

*E-mail: sabithoroz@siirt.edu.tr

can be determined through the application of dopants and various preparation techniques. For example, ZnS may show paramagnetic and ferromagnetic behavior [14–16]. To our best knowledge, no study investigating the structural, optical, magnetic and photovoltaic properties of Mn doped Sb_2S_3 TFs exists.

Several well-known methods are employed to synthesize TFs and NPs. Chemical bath deposition (CBD), which is a relatively simple and inexpensive technique, is thought to be one of the most suitable methods [17]. Unlike other methods which require intensive laboratory conditions, the CBD allows TFs to be prepared using a modest laboratory apparatus within a few hours.

In this study, Mn-doped Sb_2S_3 TFs were synthesized at room temperature using the CBD method and their structural, optical, morphological, magnetic and photovoltaic properties have been investigated for the first time with an emphasis on studying the effect of Mn content on their magnetic and photovoltaic characteristics.

2. Experimental

In order to synthesize Mn-doped Sb_2S_3 TFs at room temperature using CBD method, commercial antimony chloride ($SbCl_3$), manganese acetate ($Mn(CH_3COO)_2{\cdot}2H_2O$) and sodium thiosulfate ($Na_2S_2O_3{\cdot}5H_2O$) were used without any further purification. According to the standard CBD procedure, 0.65 g of $SbCl_3$ and 0.0025 g of $Mn(CH_3COO)_2{\cdot}2H_2O$ were dissolved in 10 mL of acetone. 25 mL of 1 M aqueous solution of sodium thiosulfate was added into a solution containing $SbCl_3$ and $Mn(CH_3COO)_2{\cdot}2H_2O$. The total volume of the mixture was brought to 100 mL through addition of an appropriate amount of deionized water. After obtaining a homogeneous mixture, a glass microscope slide that was cleaned using diluted hydrochloric acid, washed with double distilled water, and then dried, was vertically immersed in the Mn-doped Sb_2S_3 solution for 45 minutes. Afterwards, the substrate was removed from the chemical bath, washed well with deionized water and dried in air. The glass substrate was annealed at 350 °C for 1 h under N_2 atmosphere.

2.1. Characterization methods

The structural properties of the Mn-doped Sb_2S_3 TF were characterized using X-ray diffraction (XRD) on a Rigaku X-ray diffractometer with CuK_α ($\lambda = 154.059$ pm) radiation. Optical characterization was performed using ultraviolet-visible (UV-Vis) spectroscopy on a Perkin-Elmer Lambda 2. The incident photon to electron conversion efficiency (IPCE) and current density (J) versus voltage (V) measurements were performed by using PCE-S20 with a monochromatic light source consisting of a 150 W Xe lamp and a monochromator. For the IPCE and J-V measurements, fluorine doped tin oxide (FTO, 13 $\Omega{\cdot}sq^{-2}$) conductive glass substrate was used as a photoelectrode. The TiO_2 nanowire (NW) was coated on the FTO substrate using the doctor blade method, and then sintered at 450 °C for certain time. The Mn-doped Sb_2S_3 TF was grown on the TiO_2 NW coated FTO substrate at room temperature using the CBD, and then annealed at 350 °C for 1 h under N_2 atmosphere. The obtained annealed Mn-doped Sb_2S_3 TF grown on the TiO_2 NW coated on the FTO substrate was secured against a Cu_2S counter electrode containing polysulfide electrolyte. The magnetic susceptibility of the Mn-doped Sb_2S_3 TF was measured on a physical-property-measurement system (PPMS) from Quantum Design.

3. Results and discussion

3.1. Structural properties

The XRD patterns of undoped and Mn-doped Sb_2S_3 TFs synthesized on glass substrates at room temperature using the CBD are shown in Fig. 1.

All of the obtained diffraction peaks for the undoped and Mn doped TFs can be well indexed as the orthorhombic phase structure of Sb_2S_3. The obtained result is consistent with the standard card (ICDD 00-001-0538). No extra peaks have been observed which confirms that the Mn has been substituted in the Sb_2S_3 lattice. The formation of Mn compounds or Mn oxides have also been ruled out in Mn-doped Sb_2S_3 TF.

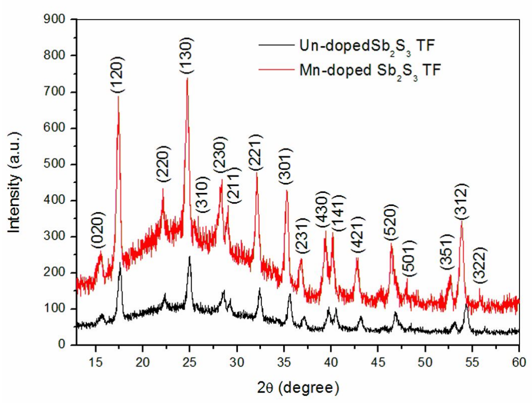

Fig. 1. The XRD patterns for undoped and Mn-doped Sb_2S_3 TFs.

The diffraction peaks of TFs prepared at room temperature were used to determine interplanar spacing (d) using Bragg's law as provided in equation 1:

$$d = \lambda/2 \cdot sin\theta \tag{1}$$

where, d is the lattice spacing, λ is wavelength of the used X-ray, and θ is the Bragg's diffraction angle. The calculated d values are collected in Table 1.

The lattice constants a, b and c have been calculated using the relation given below:

$$(1/d^2) = (h^2/a^2 + k^2/b^2 + l^2/c^2) \tag{2}$$

The obtained lattice parameters are shown in Table 2. The lattice parameters for the Mn-doped Sb_2S_3TF are in good agreement with the undoped Sb_2S_3 TF.

As can be seen in Table 1 and Table 2, the diffraction peak comes from the plane (1 3 0), whereby the Mn-doped Sb_2S_3 TF peak is slightly shifted towards a lower angle compared with those of the undoped Sb_2S_3 TF. This result suggests that the Mn has been included into the lattice of the Sb_2S_3 crystal, resulting in a change of the lattice constants.

The grain size of the TFs was estimated from the width of the relatively strong (1 3 0) diffraction peak using Scherrer formula as given in equation 3:

$$t = 0.9\lambda/(\beta cos\theta) \tag{3}$$

where t is the mean size of the TFs, λ is the wavelength of X-ray, β is the broadening measured as the full width at half maximum (FWHM) in radians, and θ is Bragg's diffraction angle. The sizes of undoped and Mn-doped Sb_2S_3 TFs determined from the XRD peak width, are 69.3 nm and 72.9 nm, respectively. This result, which is consistent with the investigations of Mushtaq et al. [12], shows that the Mn incorporation results in an increase in particle size.

3.2. Optical properties

UV-Vis spectroscopy was used to determine the band structures of undoped and Mn-doped Sb_2S_3 TFs prepared using the CBD at room temperature. The goal of the optical studies of the TFs in our present study was to make comparison between undoped and Mn-doped Sb_2S_3 TFs, as well as to show how the band gap of the Sb_2S_3 TF has changed after it was doped with Mn content. The optical absorbance spectra of undoped and Mn-doped Sb_2S_3 TFs prepared at room temperature are shown in Fig. 2.

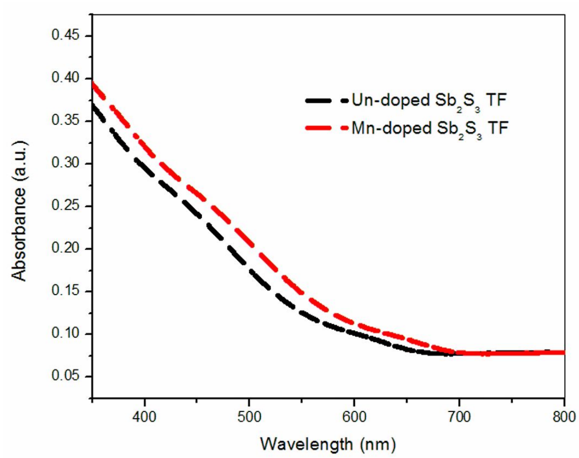

Fig. 2. The optical absorbance spectra of undoped and Mn-doped Sb_2S_3 TFs.

It can be observed that the absorption edge of the Mn-doped Sb_2S_3 TF shifts towards higher wavelengths (red shift). This means that the band gap of Mn-doped Sb_2S_3 TF decreases due to Mn content.

Table 1. Comparison of the standard and calculated d values for undoped and Mn-doped Sb_2S_3 TFs.

2 θ [degree]	Standard d value for Sb_2S_3 [Å]	Calculated d value of undoped Sb_2S_3	Calculated d value of Mn-doped Sb_2S_3	(h k l)
24.94°	3.567	3.570	–	(1 3 0)
24.76°	3.567	–	3.595	(1 3 0)

Table 2. Lattice parameters for undoped and Mn-doped Sb_2S_3 TFs.

Lattice parameters for (1 3 0)	Undoped Sb_2S_3 [Å]	Mn-doped Sb_2S_3 [Å]
a	11.28	11.25
b	11.19	11.23
c	3.82	3.86

The Tauc relation provided below was used to determine the energy band gap (E_g) of the TFs:

$$\alpha h\upsilon = C(h\upsilon - E_g)^n \quad (4)$$

where α is the absorption coefficient, n = 1/2 or 2 for direct or indirect allowed transition, respectively, C is the characteristic parameter for the respective transitions, hυ is photon energy and E_g is the energy band gap. Fig. 3 shows the plot of $(\alpha h\upsilon)^2$ versus hυ for the undoped and Mn-doped Sb_2S_3 TFs.

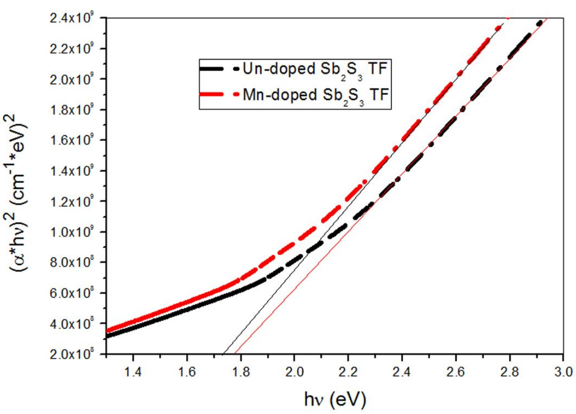

Fig. 3. Determination of the optical band gap for the undoped and Mn-doped Sb_2S_3 TFs using $(\alpha h\upsilon)^2$ vs. hυ plot.

Using the above plot, the band gap of the Mn-doped Sb_2S_3 TF prepared at room temperature was found to be approximately 1.74 eV (∼713 nm) while the band gap of the undoped Sb_2S_3 TF prepared at room temperature was around 1.77 eV (∼700 nm). It is evident that the band gap of the Mn-doped Sb_2S_3 TF decreased due to the Mn content. The Mn content was found to cause the decrease in band gap of Sb_2S_3 TF, which markedly correlates with band tailing owing to impurities involved.

3.3. Morphological properties

The SEM images of both the undoped and Mn-doped Sb_2S_3 TFs are shown in Fig. 4a and Fig. 4b, respectively. The shape of the grains is spherical.

An important observation from the SEM measurement is that the shape of Mn-doped Sb_2S_3 TF shows greater uniformity than its undoped counterpart.

An energy dispersive X-ray (EDX) spectrum was used to confirm the elemental compositions of the Mn-doped Sb_2S_3 TF. The peaks obtained from the EDX spectrum (shown in Fig. 5) are associated with Sb, S and Mn. Based on the EDX spectrum, the Sb:S:Mn molar ratio was established using the peak areas, and determined to be 40.21:57.82:1.97. This result shows that Mn was successfully doped into Sb_2S_3 TF.

3.4. Magnetic properties

The magnetic susceptibility as a function of temperature for the Mn-doped Sb_2S_3 TF measured using PPMS is shown in Fig. 6a. This sample exhibits paramagnetic behavior. The inverse of the magnetic susceptibility versus temperature is

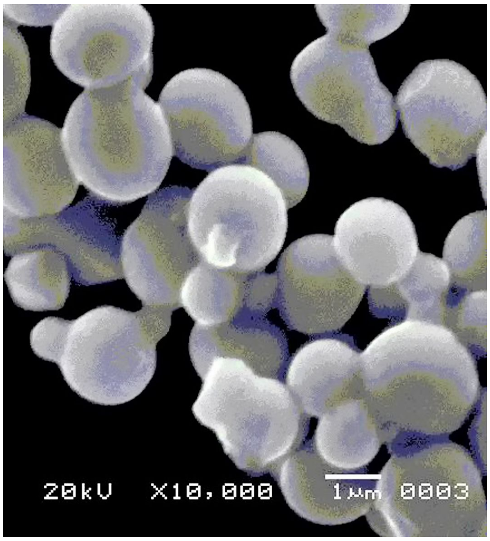

(a)

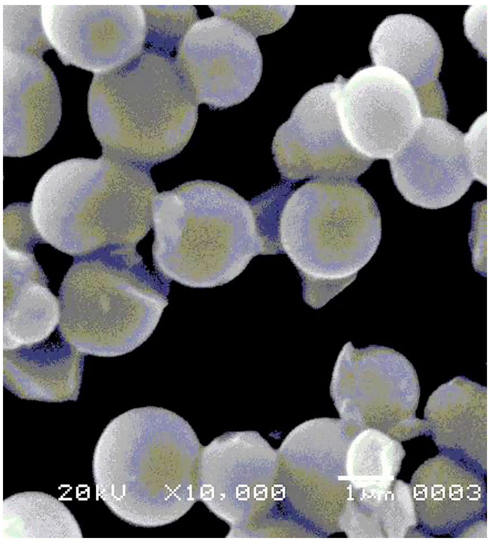

(b)

Fig. 4. SEM images of (a) undoped Sb_2S_3 TF, (b) Mn-doped Sb_2S_3 TF.

shown in Fig. 6b. The paramagnetic Curie-Weiss temperature was found to be -4.1 K by linear fitting the experimental data to the Curie-Weiss law. This result suggests that there is anti-ferromagnetic interaction between the Mn moments in the Mn-doped Sb_2S_3 TF.

3.5. Photovoltaic properties

Fig. 7 demonstrates the incident photon to electron conversion efficiency (IPCE) spectra for

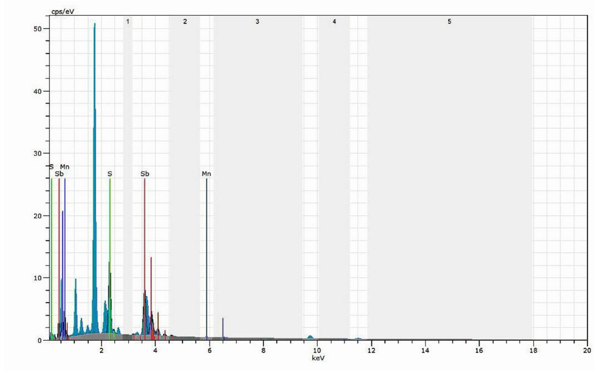

Fig. 5. EDX spectrum of the Mn-doped Sb_2S_3 TF synthesized at room temperature.

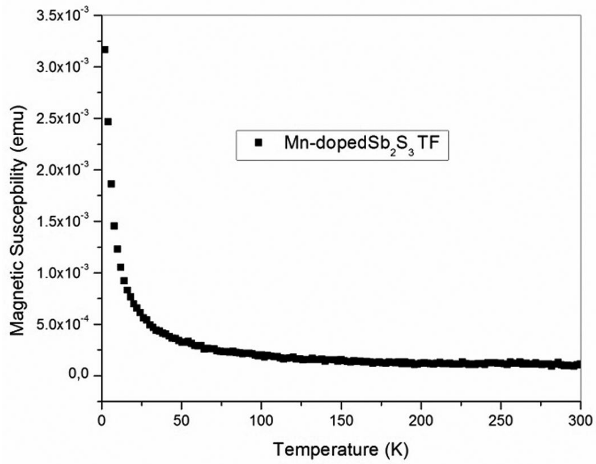

(a)

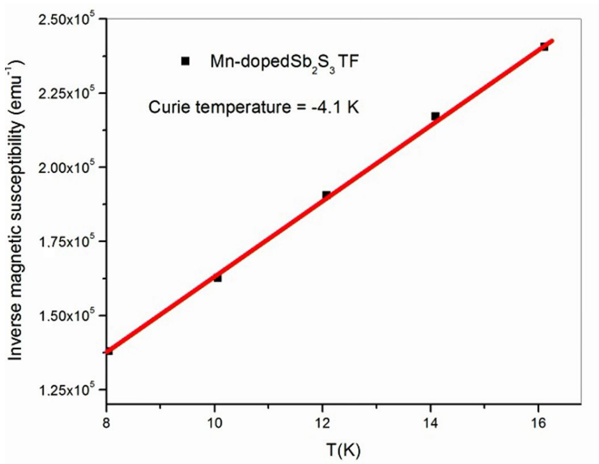

(b)

Fig. 6. (a) Magnetic susceptibility versus temperature, (b) inverse magnetic susceptibility vs. temperature for the Mn-doped Sb_2S_3 TF prepared by the CBD method at room temperature.

devices fabricated from undoped and Mn-doped Sb_2S_3 TFs. Initially, the IPCE value of the undoped Sb_2S_3 TF shows an increase with Mn content. The obtained maximum IPCE value is 55.7 % for Mn-doped Sb_2S_3 TF while the value of 51.3 % is maximum for undoped Sb_2S_3 TF. It can be clearly seen that Mn content plays an important role to increase the IPCE value of the Sb_2S_3 TF.

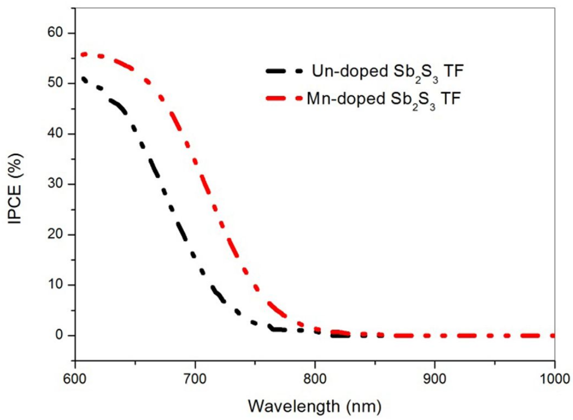

Fig. 7. The IPCE spectra of undoped and Mn-doped Sb_2S_3 TFs attached to TiO_2 NWs.

The current density (J) versus voltage (V) plot for undoped and Mn-doped Sb_2S_3 TFs attached to TiO_2 NWs is shown in Fig. 8. It is important to note that there is a significant improvement in the performance of the Mn-doped Sb_2S_3 TF solar cell prepared at room temperature when compared with the undoped Sb_2S_3 TF solar cell. The power conversion efficiencies were obtained as 6.15 % and 5.57 % for Mn-doped and undoped Sb_2S_3 TFs prepared at room temperature, respectively. Open circuit voltage (V_{OC}), short circuit current density (J_{SC}), fill factor (FF), and power conversion efficiency (η%) are shown in Table 3.

The reasons for this improvement could be as follows: (a) the Mn-doped Sb_2S_3 TF has an enhanced spectral response compared to the undoped Sb_2S_3 TF, which can result in enhancement in the current density, (b) the grain size of the Mn-doped Sb_2S_3 TF increases due to the Mn which causes a reduction in the particle to particle hopping of the photo-induced carriers, (c) the contact between the Mn-doped Sb_2S_3 TF and TiO_2 NW is improved because of the Mn content. This positive contact is able to block the interfacial recombination of the injected carriers from NWs to polysulfide electrolytes, which hence will improve the performance of the Mn-doped Sb_2S_3 TF solar cells.

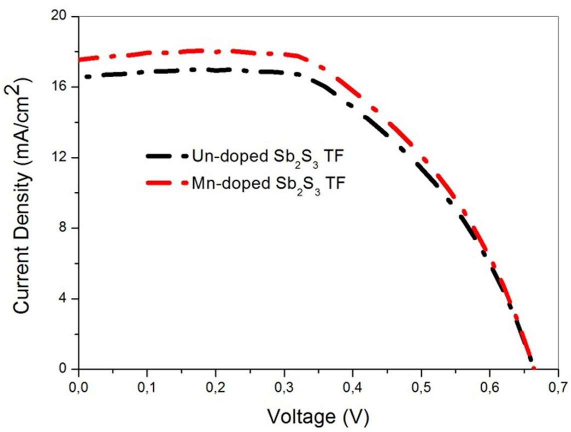

Fig. 8. J-V plots of undoped and Mn-doped Sb_2S_3 TFs attached to TiO_2 NWs.

4. Conclusions

In our present study, Mn-doped Sb_2S_3 TFs were synthesized at room temperature using the CBD method. Their structural, optical, morphological, magnetic and photovoltaic properties have been investigated for the first time. XRD study of structural properties has shown that all of the obtained diffraction peaks for both the undoped and Mn doped TFs prepared at room temperature can be suitably indexed as the orthorhombic phase structure of Sb_2S_3 and that the grain size of the Mn-doped Sb_2S_3 TF (72.9 nm) becomes larger than that of undoped Sb_2S_3 TF (69.3 nm) due to the presence of Mn dopant. The optical study (optical absorption) revealed that the band gap of Mn-doped Sb_2S_3 TF decreases because of the Mn doping. It was observed that Mn doping causes this decrease, which, in turn, points to band tailing owing to the impurities involved. The morphological study showed that the shape of the Mn-doped Sb_2S_3 TF is more uniform than the shape of its undoped counterpart. The study on the magnetic properties demonstrated that the Mn-doped Sb_2S_3 TF exhibits paramagnetic behavior. A paramagnetic Curie-Weiss temperature

Table 3. Comparison of V_{OC}, J_{SC}, FF, and η% values for undoped and Mn-doped Sb_2S_3 TFs attached on the TiO_2 NWs.

TFs	V_{OC} [V]	J_{SC} [mA/cm^2]	FF	η%
Un-doped Sb_2S_3	0.66	16.55	0.51	5.57
Mn-doped Sb_2S_3	0.66	17.58	0.53	6.15

was determined as −4.1 K, suggesting that there is anti-ferromagnetic interaction between the Mn moments in the Mn-doped Sb_2S_3 TF. The IPCE and J-V measurements, carried out for the Mn-doped Sb_2S_3 TF for the first time in this study, showed that the Mn-doped Sb_2S_3 TF can be utilized as sensitizers to improve the performance of solar cells. The power conversion efficiency (η%) was obtained as 5.57 and 6.15 for undoped and Mn-doped Sb_2S_3 TFs, respectively. Our study suggests that introduction of dopant could serve as an effective means of improving the overall device performance of solar cells.

References

[1] GROZDANOV I., *Semicond. Sci. Tech.,* 9 (1994), 1234.

[2] FORGUE S.V., GOODRICH R.R., COPE A.D., *RCA Rev.,* 12 (1951), 335.

[3] ARUN P., VEDESHWAR G., *J. Mater. Sci.,* 31 (1996), 6507.

[4] KRISHNAN B., ARATO A., CARDENAS E., *Appl. Surf. Sci.,* 254 (2008), 3200.

[5] KYONO A., KIMATA M., MATSUHISA M., MIGASHITA Y., OKAMOTO K., *Phys. Chem. Miner.,* 29 (2002), 254.

[6] VERSAVEL M.I., HABER J.A., *Thin Solid Films,* 515 (2007), 7171.

[7] HONGWEI L., GUANG Y., YAXIONG G., LIANGBIN X., PINGLI Q., XIN D., XIAOLU Z., WEIJUN K., HONG T., ZHAO C., BORUI L., GUOJIA F., *Phys. Chem. Chem. Phys.,* 18 (2016), 16436.

[8] TZOFIA E., EYAL T., LIOZ E., *J. Phys. Chem. C.,* 119 (2015), 12904.

[9] YAHUITL O.M., THOMAS P.W., RONGPING W., ZHIYONG Y., KYLIE R.C., *Phys. Status Solidi A,* 213 (2015), 108.

[10] YONG C.C., DONG U.L., JUN H.N., EUN K.K., *Adv. Funct. Mater.,* 24 (2014), 3587.

[11] ZHONG J., XIAOJIAN Z., YONGJIA Z., MAN Z., MINGJU W., SUJUAN W., JINWEI G., XINGSEN G., JUN-MING L., HONGBO Z., *ACS Appl. Mater. Inter.,* 5 (2013), 8345.

[12] MUSHTAQ S., BUSHRA I., MUHAMMAD R., AURANG Z., *Nat. Sci.,* 8 (2016), 33.

[13] CHEN W., MALM J.O., ZWILLER V., HUANG Y., LIU S., WALLENBERG R., BOVIN J.O., SAMUELSON L., *Phys. Rev. B.,* 61 (2000), 11021.

[14] REN G., LIN Z., WANG C., LIU W., ZHANG J., HUANG F., LIANG J., *Nanotechnol.,* 18 (2007), 035705.

[15] SAMBASIVAM S., JOESPH D.P., LIN J.G., VENKATESWARAN C., *J. Solid State Chem.,* 182 (2009), 2598.

[16] LAKSHMI P.V.B., RAJ K.S., RAMACHANDRAN K., *Cryst. Res. Technol.,* 44 (2009), 153.

[17] LAZOS C.G., ROSENDO E., JUÁREZ H., SALGADO G.G., DIAZ T., FALFÁN M.R., OLIVA A.I., QUINTANA P., AGUILAR D.H., CAUICH W., *J. Electrochem. Soc.,* 155 (2008), 158.

Received 2017-07-07
Accepted 2017-12-06